Spectroscopic studies of rubidium vapour zone produced by thermal evaporation in noble gas

1999 J. Phys.: Condens. Matter 11 6605

(http://iopscience.iop.org/0953-8984/11/34/313)

J. Phys.: Condens. Matter **11** (1999) 6605–6619. Printed in the UK PII: S0953-8984(99)03058-1

Spectroscopic studies of rubidium vapour zone produced by thermal evaporation in noble gas

Shosuke Mochizuki†, Ken-ichi Inozume‡ and Raphael Ruppin§

Department of Physics, College of Humanities and Sciences, Nihon University, 3-25-40 Sakurajosui, Setagaya-ku, Tokyo 156-8550, Japan

E-mail: motizuki@physics.chs.nihon-u.ac.jp

Received 29 March 1999

Abstract. The time evolution of the extinction spectra of the rubidium vapour zone has been measured during the process of gas evaporation. The structure of the spectra and their time dependence show the occurrence of atoms, dimers, clusters and microcrystals. Also, they show a size trend in the surface plasma resonance frequency of rubidium clusters.

Also, vapour species in each zone were selectively excited by using laser light and the emission spectra were measured.

Some of the observed spectra were compared with theoretical ones, and information on the following points was derived: (1) the mechanism of rubidium cluster and microcrystal growth in the gas evaporation method, (2) the size trend of the collective mode resonance of the valence electrons, (3) the excitation energy transfer between rubidium vapour species, (4) the structure of the vapour zone and (5) the mechanism of laser photofragmentation of clusters.

1. Introduction

There have been a considerable number of studies on the optical properties of alkali-metal vapours as a possible source of a tunable high power laser and as a simple system for the investigation of the formation of the collective nature of valence electrons with an increasing number of constituent atoms (Brechignac *et al* 1992). Mann and Broida (1973) studied the optical scattering spectra of various kinds of alkali-metal vapour in steady state in gas evaporation and obtained the surface plasmon absorption spectra of sodium and potassium microcrystals. Also, they reported that the resonant scattering behaviour of rubidium was difficult to obtain. By the way, the optical properties of rubidium aggregates, together with those of caesium ones, are of special interest, because solid rubidium is at the boundary of applicability of the nearly-free electron model, since it has a d-like band near the Fermi surface. Moreover, rubidium vapour shows amplified spontaneous orange band emission which is potentially important as a continuously tunable excimer-type laser source (Xing *et al* 1992).

Recently, both by setting an appropriate condition for gas evaporation and by measuring the time and space evolutions of the optical spectra of the rubidium vapour zone during gas evaporation in low pressure helium gas, we showed that atoms evaporate first and then some of the rubidium atoms aggregate to produce dimers and clusters (Mochizuki 1993). Moreover, we have deduced size trends in optical properties of rubidium clusters from the observed

‡ Present address: 1st R&D Department, Teraoka Seiko Co., Ltd, 5-13-12 Kugahara, Ohta-ku, Tokyo 146, Japan.
§ Present address: Department of Physics and Applied Mathematics, SOREQ NRC, Yavne 81800, Israel.

0953-8984/99/346605+15$30.00

time evolution. Here we describe further, more detailed measurements on rubidium vapour, and various atmosphere gases. Very recently, we have carried out such measurements on rubidium vapour under various atmosphere gases in more detail. Also, we excited selectively dimers and clusters in rubidium vapour zones by laser light and measured the emissions from them. The results gave information on the interaction and excitation energy transfer between vapour species. With increasing laser fluence, the photofragmentation phenomenon becomes prominent. As observed in the photofragmentation of the vapour zones of sodium and potassium (Mochizuki and Tsumura 1998), we have also observed the rubidium diffuse bands which may arise from dissociation of rubidium trimers to produce excimer-like dimers. Such photofragmentation spectroscopy may give more detailed information on the vapour zones, which complements what the extinction measurements give.

In the present paper, we present in detail the time evolution of the extinction spectra of rubidium vapour during thermal evaporation in various atmospheres. Some of the observed spectra were compared with theoretical ones. The results provide information on the growth process of dimers and on the size trend of the surface plasma resonance frequency of the rubidium clusters and microcrystals. Also, the experiments on the laser-induced photoluminescence and photofragmentation of rubidium vapour are reported and discussed.

2. Experiment

2.1. Gas evaporation experiments

The experiments were carried out using the apparatus described in our previous papers (Mochizuki 1991, 1993, Mochizuki and Ruppin 1993, 1994). A Pyrex glass crucible containing rubidium metal was indirectly heated in an alumina crucible on which a tungsten-wire heater was wound. The temperature of the glass crucible was gradually increased by applying a constant voltage. Prior to optical measurements, the temperatures of the crucible and of representative positions in the vapour zone were measured with a thermocouple under the same condition of gas evaporation with which the optical measurements would be made. Optical spectra of selected positions in the vapour zone were recorded in a transmission configuration as a function of the time elapsed from the beginning of the evaporation. Continuum light from a 150 W Xe lamp was directed at the whole vapour zone above the crucible through the optical window without using a lens. After passing the vapour zone, only the light through a selected position was collected by lens and then spectrally analysed and recorded by an optical multichannel analyser system. The transmission at a given height is the intensity ratio of the transmitted radiation during the evaporation process to that of the transmitted radiation through the same position before the beginning of the gas evaporation. Since the transmission spectra T_r obtained contain the effects of both scattering and absorption, the results are expressed with respect to the extinction spectra $-\log T_r$.

2.2. Laser-induced luminescence and fragmentation experiments

The laser induced emission experiments were carried out by using a dye laser excited by a nitrogen laser (pulse width=300 ps). The wavelengths were adjusted to the X–B absorption band of rubidium dimers. The diameter of the laser spot was about 0.6 mm. The laser induced fragmentation experiments were carried out by using an Nd^{3+}–YAG laser line ($\lambda = 1.06\ \mu$m, fluence=200 mJ cm^{-2}, pulse width=10 ns) on rubidium vapour produced by gas evaporation. The diameter of the laser spot was about 0.6 mm. The emitted light was dispersed using a grating spectrograph (Jobin–Yvon HR-320) and a multichannel-photo-detection system was

employed. After an intense laser light pulse, the emissions from the target vapour were recorded in the right-angle scattering configuration, with an integration time of 1 s. The integration was started just before the laser irradiation.

3. Results and discussion

3.1. Optical extinction spectra of rubidium vapour

Figure 1(a) shows the time evolution of the extinction spectrum of the vapour zone at a height of 6 mm from the crucible edge. The evaporation was carried out at confined pressure of 140 Torr. During the gas evaporation, the temperature of the vapour zone rose to 573 K. The time-resolved spectrum consists of 32 spectra. The 30th spectrum is shown in figure 1(b). At the initial stage of evaporation, only four sharp absorption lines, L_1 (about 795 nm), L_2 (about 780 nm), L_3 (about 420 nm) and L_4 (about 360 nm), are seen. These wavelengths are close to the reported values (White 1934, Lide 1990–1991, Phelps 1982) of the S–P electronic transitions in atomic rubidium Rb_1. Although these absorptions are due to transitions from S to two P levels split by spin–orbit interaction, only the absorption due to transitions to 5P states is resolved because we are using a wide-wavelength-range optical multichannel analyser (spectral resolution of 0.6 nm), which prevents an absolute determination of the relevant wavelengths. With progressive gas evaporation, broad absorption bands appear at about 675, 473, 432, 373 and 348 nm. By referring to a spectroscopic table (Rosen 1970), the 675, 473 and 432 nm bands are assigned to the X–B, X–C and X–D electronic–vibrational transitions in rubidium dimer Rb_2, respectively. However, the 373 and 348 nm bands are not shown in the table. A careful study of their time dependence shows that these bands appear simultaneously with the X–D and X–C transitions, which allows us to assign them to transitions from the ground state (X) to other higher states in Rb_2. Also, the sharp absorption lines L_5 (about 333 nm), L_6 (about 322 nm) and L_7 (about 313 nm) are seen, which are due to the S–P electronic transitions in Rb_1: these wavelengths differ slightly from reported values (White 1934, Lide 1990–1991, Phelps 1982), because we are using a wide-wavelength-range optical multichannel analyser (spectral resolution of 0.6 nm). Figure 1(c) shows the time dependences of peak values of the extinctions (absorption) due to Rb_1 and Rb_2. Since the spectra were considerably affected by some background extinction, we subtracted it from each observed extinction value. The background extinction may arise both from the X–A transition of Rb_2 and from rubidium clusters. Since each extinction is proportional to the number for Rb_1 and Rb_2, respectively, the curve shows the time dependence of numbers. The number of Rb_1 increases with time and then, after reaching a maximum, begins to decrease, while the number of Rb_2 begins to increase with some time lag behind Rb_1 and continues to increase. This may indicate that Rb_2 is produced by coalescence of Rb_1. Also, we note that, since no emission is observed from the vapour zone without illumination, the dimers are cooled not by photoemission but by collisions with helium gas atoms. It is also noted that, in figure 1(b), a weak broad band DB is similar to the orange emission diffuse band observed in the dense rubidium vapour produced by the heat-pipe oven method (Pichler *et al* 1983). Such a diffuse band appears at the short-wavelength end of the X–B alkali dimer band system. For the formation of the diffuse band, the dissociative recombination

$$Rb_3^+ + e \rightarrow Rb_1 + \text{ excimer-like } Rb_2 \qquad (1)$$

has been proposed.

The above-shown spectra are those for dense vapour. It has been said that, even in vacuum evaporation, rubidium vapour contains not only atoms but also dimers. However, it is not clear whether dimers come from the liquid surface or atoms coalesce to produce dimers in the vapour

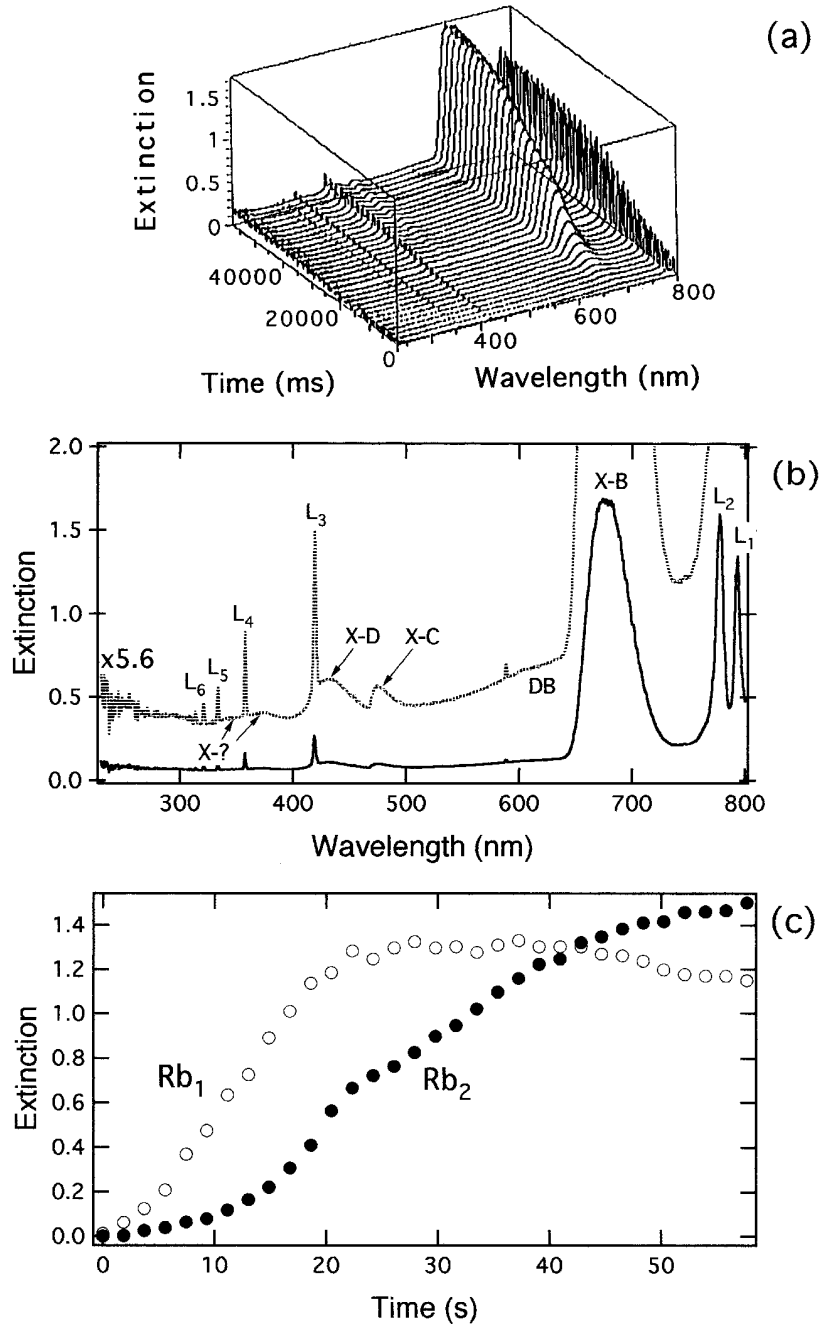

Figure 1. (a) Time evolution of extinction spectrum of dense rubidium vapour zone under helium atmosphere, (b) 30th spectrum of the time-resolved spectra (a). The upper curve shows a magnification of the lower one by a factor of 5.6. (c) Time dependences of the extinctions due to rubidium atoms and dimers.

phase. Therefore, in order to clarify this point, we studied the optical spectra of a thin rubidium vapour zone. We have evaporated rubidium both in helium and argon gas confined at 140 Torr

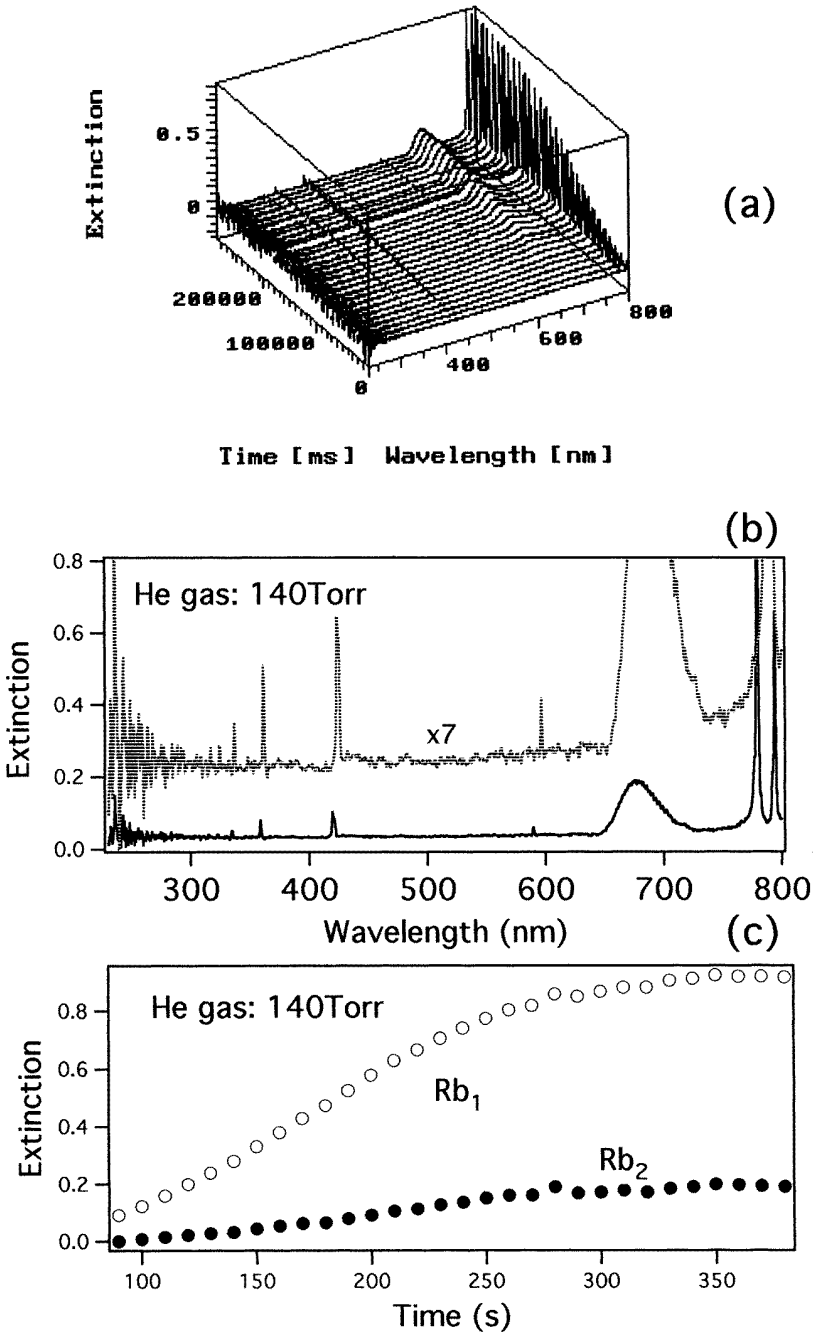

Figure 2. (a) Time evolution of extinction spectrum of thin rubidium vapour zone under helium atmosphere, (b) 30th spectrum of the time-resolved spectra (a). The upper curve shows a magnification of the lower one by a factor of 7. (c) Time dependences of the extinctions due to rubidium atoms and dimers.

by applying the same voltage to the alumina crucible heater. The voltage was about one half of that for the dense vapour evaporation described above. The results are shown in figures 2 and 3.

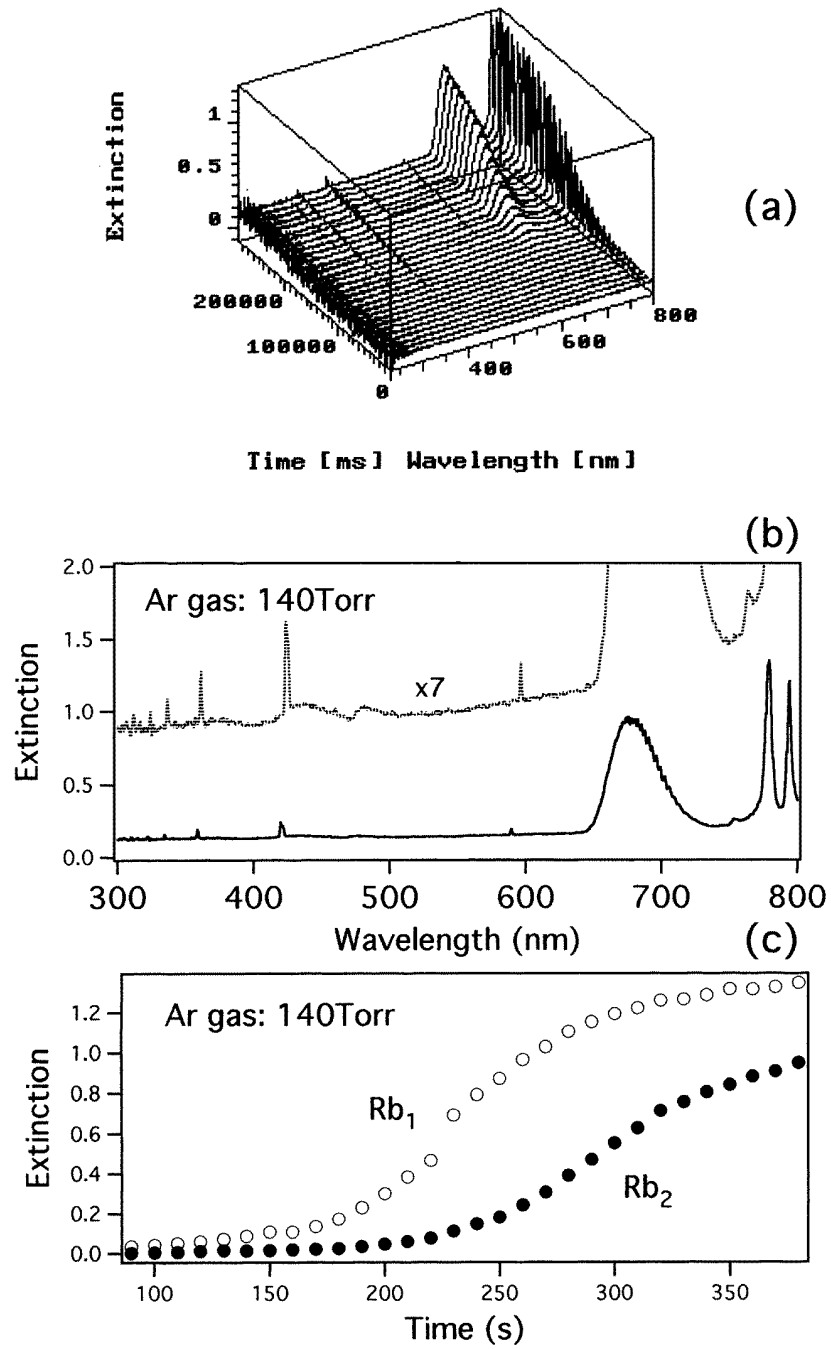

Figure 3. (a) Time evolution of extinction spectrum of thin rubidium vapour zone under argon atmosphere, (b) 30th spectrum of the time-resolved spectra (a). The upper curve shows a magnification of the lower one by a factor of 7. (c) Time dependences of the extinctions due to rubidium atoms and dimers.

Both the spectral evolutions with time are similar to that observed under the dense evaporation

condition. As seen from these figures, surely, atoms first appear and then dimers appear with some time lag behind Rb_1 and continue to increase in number. This again may indicate that rubidium dimer is produced by coalescence of two rubidium atoms. However, depending on the kind of atmospheric gas, the following differences are seen in the time dependences of the extinction intensities for atom and dimer as shown in figures 2(c) and 3(c). The plotted extinction values are raw values, not ones subtracted by background extinction. During the gas evaporations in helium and argon gas, the ratio of Rb_2 extinction to Rb_1 extinction varied from 0.005 to about 0.21, and from 0.05 to 0.69, respectively. These ratio increases with time may indicate also that rubidium dimer is produced by coalescence of two rubidium atoms. The difference of the experimental results for two kinds of atmospheric gas are as follows.

(1) Under helium gas atmosphere, atoms and dimers appear at an earlier stage of the evaporation than under argon atmosphere,
(2) At the final stage of evaporation, the extinction intensities of atoms and dimers are larger under the argon atmosphere than under the helium one. Also, the extinction intensity ratio of dimer to atom is larger under the argon atmosphere than under the helium one.

The result (1) arises from a difference in the temperature elevation speed of the crucible heater, depending on the kind of atmospheric gas. Temperature variation of the vapour zone with time was measured with a thermocouple. The results are shown in figure 4. However, at the final stage of evaporation, the temperature was nearly independent of the kind of atmospheric gas. Therefore, the result (2) may arise mainly from difference of mean free path of evaporated atoms, depending on the mass of atmospheric gas, which means that a heavier atmospheric gas promotes easier aggregation, as observed previously for lithium evaporation (Mochizuki *et al* 1997).

3.2. Surface plasmon resonance in rubidium microcrystals

From gas-evaporation experiments on various types of metal, we know that free large metal clusters and microcrystals can be produced by evaporation in a moderate pressure gas stream. Smaller clusters appear, of course, at an earlier stage of the gas evaporation. Figure 5(a) shows the time evolution of the extinction spectrum of the rubidium vapour zone at a height of 58 mm from the crucible edge. Spectra 1, 2, 3 and 4 were measured at 40.8, 41.5, 42.2 and 42.9 s after the beginning of melting, respectively. The evaporation was carried out in a stream of helium gas with a pressure of 2 Torr and a flow rate of 0.5 l min^{-1}. During the gas evaporation, the temperature of the crucible rose to 573 K. Unfortunately, we could not determine the sizes and shapes of the clusters or microcrystals by transmission electron microscopy on the collected microcrystals, because of the high reactivity with the atmospheric moisture. As shown in this figure, at the beginning stage of gas evaporation, a very broad band is observed at about 730 nm, together with sharp lines due to Rb_1: spectrum 1. Then, the broad band becomes a double-peaked structure of which the peaks are at about 630 and 730 nm: spectrum 2. With further progress of gas evaporation, the short-wavelength band grows to make a clear single-peak band and shifts to a shorter wavelength with time: spectra 3 and 4. The peak shifts as far as 621 nm with decreasing band width. The observed bands which shift to shorter wavelength with time are due to the surface plasma resonance absorption in rubidium clusters. Since cluster growth proceeds with time in our experiment, the observed time trend can be supposed to be the size trend, though there is some size distribution in the vapour zone. The time trend of the peak shift is similar to that of sodium clusters (Mochizuki 1992) and also to the size trend of the peak shift in potassium cluster ions (Brechignac *et al* 1992). The broadness of the spectra for the smallest sizes may be attributed to the presence of non-spherical clusters. Thus,

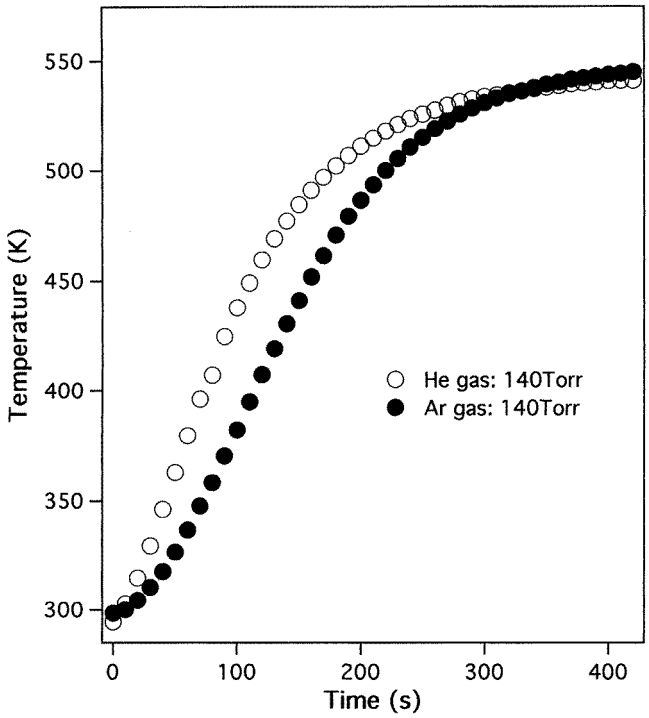

Figure 4. Temperature variation of rubidium vapour zone under helium and argon atmospheres.

for an ellipsoidal cluster, the single absorption peak of the sphere splits into three peaks. Such a splitting has been observed, e.g. for very small sodium clusters (Selby *et al* 1989, 1991). With increasing cluster size, the spherical shape predominates, and the blueshift of the peak with increasing size is due to the electron spillout effect (Brechignac *et al* 1992). This spillout effectively reduces the electron density in small clusters, leading to a lowering of the resonance frequency. With increasing size, the spillout decreases in magnitude, so that the resonance frequency shifts towards the blue, as seen in figure 5(a). Taking into account such an electron spillout effect, the resonance frequency ν_s' and the electron spillout parameter of monovalent metals are related by

$$\nu_s' = \nu_s[1 + (\delta/r_s)n^{-1/3}]^{-3/2} \tag{2}$$

$$\nu/r_s n^{1/3} = \delta^* = (\nu_s/\nu_s')^{2/3} - 1 \tag{3}$$

$$\nu_s = (1/2\pi)(e/m^* r_s^3)^{1/2} \tag{4}$$

where ν_s is the resonance frequency without such an electron spillout correction, m^* is the electron effective mass, r_s is the Wigner–Seitz radius of bulk, δ^* is the normalized electron spillout parameter and n is the total number of valence electrons. The normalized electron spillout parameter δ^* is estimated from the above equations using m^*, r_s (Ashcroft and Mermin 1976) and the measured resonance frequency. However, the thus obtained ν_s' and δ^* are extraordinarily large because an effect due to ionic core polarization is ignored in the above expression. Therefore, we have regarded the observed maximum resonance frequency 4.828×10^{14} Hz(= 621 nm) as ν_s in equation (2) and then obtained the normalized electron spillout parameters of 0.114, 0.009 and 0.002 for spectra 1, 2 and 3, respectively.

To see the time evolution at a later evaporation stage than that of figure 5(a), another

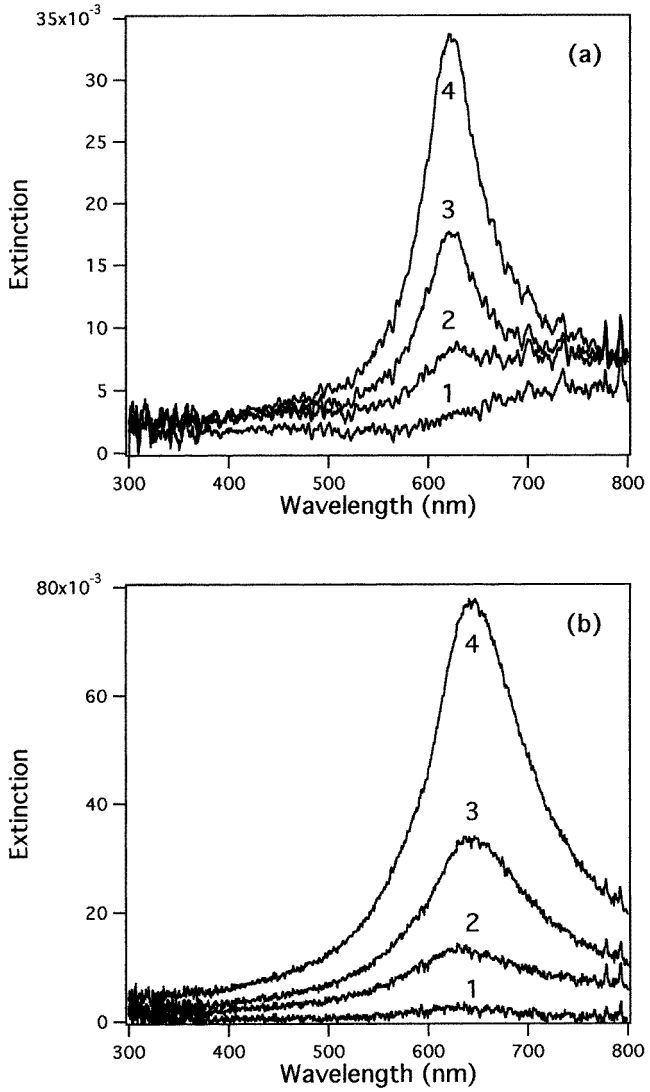

Figure 5. Time evolution of rubidium vapour zone under flowing gas condition. (a) rapid evaporation condition, (b) slow evaporation one.

measurement was carried out under the same gas evaporation condition, but the time intervals between the successive measurements were much longer. During the gas evaporation, the temperature of the crucible rose to 600 K. The result is shown in figure 5(b). Spectrum 1 corresponds nearly to spectrum 4 of figure 5(a). Spectra 2, 3 and 4 were measured at 35.4, 55.1 and 86.6 s after the measurement of spectrum 1, respectively. As shown in the figure, after reaching a certain stage of gas evaporation, the blueshifted surface plasma resonance peak begins to go back to a longer wavelength (up to about 640 nm) and to increase its width. The redshifted frequency and the broadening with increasing size can be explained by calculating the size dependence of the Mie scattering cross section of a spherical particle. However, since we have no method for determining the sizes of such free microcrystals *in situ*, we estimated the

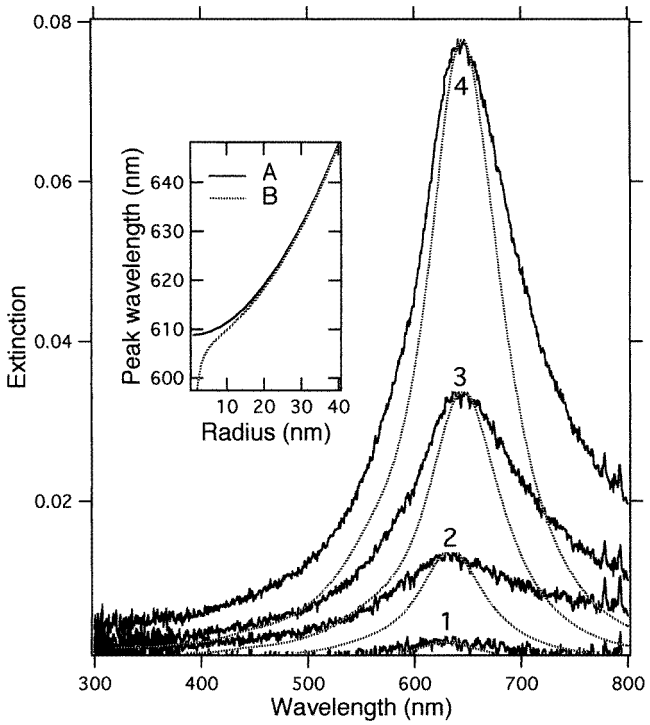

Figure 6. Calculated extinction cross sections (smooth broken curves) of rubidium spheres of radii 24, 29, 32 and 39 nm, the peaks of which coincide with those of the experimental spectra (solid curves) shown in figure 5(b). The extinction intensity peak wavelength calculated is plotted as a function of sphere radius in the inset. Curves A and B are obtained with and without the size dependent correction of the free path effect, respectively.

sizes by fitting to calculated extinction cross sections of spherical microcrystals, as in previous studies (Mochizuki and Ruppin 1993, 1994). For these calculations, we have employed the values of the frequency dependent dielectric complex constant of rubidium as measured by Smith (1970). These, however, refer to the bulk, and for small spheres have to be so as to account for the free-path effect, which leads to an increase of the imaginary part of the dielectric constant. For this size dependent correction, the form suggested by Kreibig (1974) has been used. In the calculation, we have varied the sphere size, until the peak positions agreed with those of curves 2, 3 and 4 of figure 5(b). Since the number of the microcrystals contributing to the extinction is not known, we have scaled the theoretical curves, so that the heights of the maxima coincide with the experimental ones. The results, shown in figure 6, indicate that the microcrystals had an average radius of about 24 nm (curve 1) at the initial stage, about 32 nm (curve 3) at the middle stage and 39 nm (curve 4) at the final stage. The experimental extinction spectra (solid curves) are broader than calculated ones (broken curves), because of the size and shape distributions which inevitably exist in the experiment. Also, the theoretical extinction intensity peak wavelength is plotted as a function of sphere radius in the inset of figure 6. The curves A and B are obtained with and without the size dependent correction of the free path effect, respectively. The temperature increase with progressing gas evaporation may also induce such a redshift. However, a simple estimation taking into account thermal dilation gives a much smaller shift (<3 nm) than that (19 nm) between spectra 1 and 4 of figure 5(a). It is noted that, though the time intervals between the spectra of figure 5(a) are much smaller

than those of figure 5(b), the observed growth in extinction spectrum is extraordinarily rapid at the early stage of gas evaporation. This indicates that, in the gas-flowing condition, the smaller clusters coalesce more rapidly to produce larger clusters.

Rubidium metal crystallizes in a body-centred cubic lattice. The calculation of the electronic structure of solid rubidium shows a energy gap (0.46 eV) at the symmetry point N at which electrons have S- and D-wave characters, and Fermi energy is 1.79 eV (Inoue *et al* 1971a, b, Yamashita 1973). Conduction electrons originate from S and D states and have an optical effective mass ($m^*_{opt} = 1.16\,m_0$) (Smith 1970) and a thermal one ($m^*_{th} = 1.26\,m_0$) (Lien and Phillips 1964, Filby and Martin 1965). It is of interest to deduce the electron effective mass m^* from the highest peak energy 1.997 eV (=621 nm) shown in figure 5(a), through the following expression for a spherical microcrystal:

$$\omega_r^2 = 4\pi n e^2/3m^* \tag{5}$$

where ω_r and n are the collective-mode-resonance frequency and electron density, respectively. This follows from the fact that for a free-electron-like sphere, the resonance frequency is related to the plasma frequency ω_p by

$$\omega_r = (\omega_p^2/3)^{1/2}. \tag{6}$$

The value of n was taken to be equal to 1.08×10^{22} cm^{-3} (Yamashita 1973). The value thus obtained is $m^* = 1.13\,m_0$, which is close to the reported optical one, which is not surprising, since our estimate here is also based on an optical experiment.

3.3. Selective photoexcitation of rubidium dimers in vapour

We excited rubidium dimers in the vapour zone by various lines between 640 nm and 690 nm emitted from a dye laser, and obtained the luminescence spectra. Typical results are shown as curves (a and b) in figure 7, together with the extinction spectrum. All spectra were obtained at the steady state of gas evaporation.

The condition for the gas evaporation was the same as that for thin vapour measurements. The broad emission band with sharp fine structures is due to the B–X transitions. A broad intensity dip that appeared in each spectrum is due to absorption of environmental dimers in the ground state. With decreasing wavelength of the excitation light, the B–X emission band broadens, which is the same phenomenon as for lithium vapour (Mochizuki *et al* 1997). This may be due to the anharmonicity of the adiabatic potential curves of the X and B states. The photoexcited dimers may deexcite to emit light, or to dissociate or transfer their excitation energies to nearby atoms, dimers and clusters through collisions. Therefore, under photoexcitation of dimers, atomic emission lines may be observed simultaneously. Certainly, we can see two atomic lines L_1 (about 795 nm) and L_2 (about 780 nm). The intensity ratio of the atomic emission to dimer one increases with increasing wavelength of the excitation light. The atomic emission may arise from the appearance of excited atoms due to predissociation of the excited lithium dimers in the B state and some energy transfer from the excited dimer to atom to excite the atom in the ground state, as in the following processes.

$$Rb_2(B) + \Delta E \rightarrow Rb(5S) + Rb(5P) \tag{7}$$

and

$$Rb_2(B) + Rb(5S) \rightarrow Rb_2(X) + Rb(5P). \tag{8}$$

Taking into account the potential curves calculated for Rb_2 (Brom and Broida 1974, Suemitsu *et al* 1992), the energy defect ΔE of about 2000 cm^{-1} is so large that direct photodissociation of $Rb_2(B)$ as indicated by equation (7) never occurs. However, if the potential curves of the

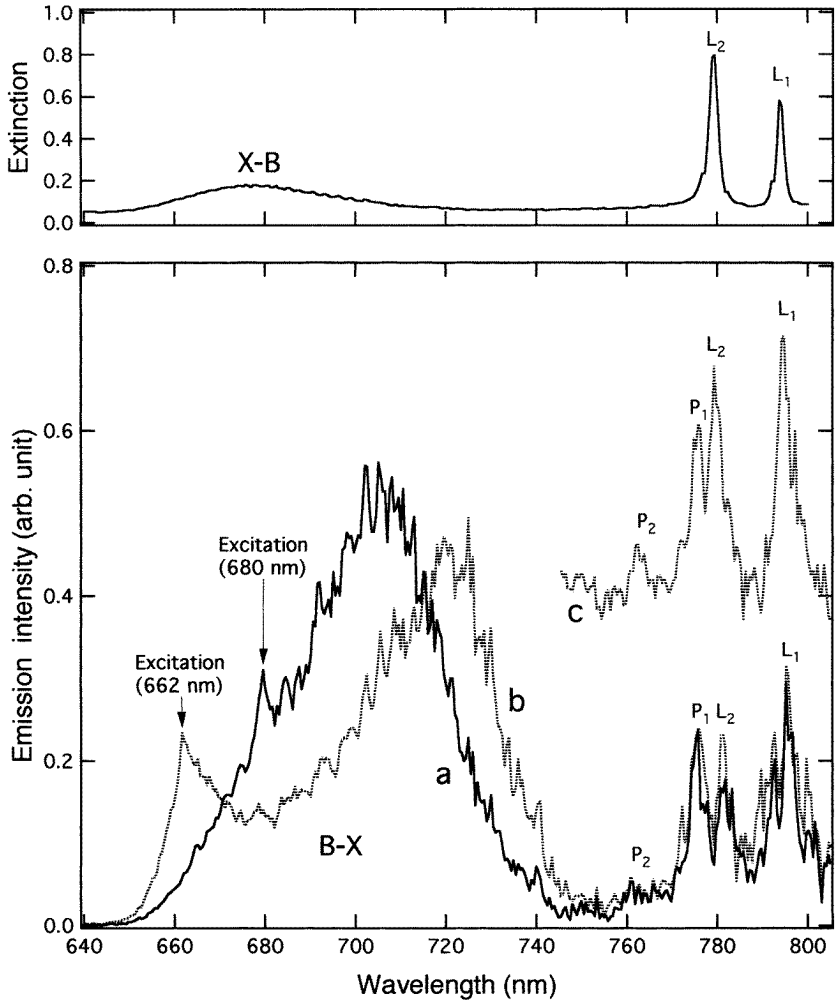

Figure 7. Photoluminescence spectra of rubidium dimers for two excitation wavelengths. Curves a and b were measured with the integration time of 1 s. The inset curve c was measured with the integration time of 10 s. The extinction spectrum is also shown in the uppermost figure.

B and A states intersect each other as reported by Brom and Broida (1974), Rb_2 in the B state may transit the A state to predissociate even by a one-photon process. On the other hand, since the potential minimum energy of the $Rb_2(B)$ is close to the energy of $Rb_1(5P)$, collisional energy transfer given by equation (8) may realize atomic emission.

Two other emission lines P_1 (about 776 nm) and P_2 (about 762 nm) are also seen in figure 7. To observe these lines clearly, we measured the emission spectra for longer integration time (10 s). The result (curve c) is inset in figure 7. These two emission lines can be assigned to the electronic transitions from $Rb_1(5D)$ to $Rb_1(5P_{3/2})$ and $Rb_1(5P_{1/2})$.

$$Rb_1(5D_{3/2}) \rightarrow Rb_1(5P_{1/2}) \text{ and } Rb_1(5D_{5/2}) \rightarrow Rb_1(5P_{3/2}). \tag{9}$$

Such an $Rb_1(5D)$ state may be produced by the following energy pooling process (Barbier and Cheret 1983) in the vapour zone,

$$Rb_1(5P_{3/2}) + Rb_1(5P_{3/2}) + 68\ cm^{-1} \rightarrow Rb_1(5D) + Rb_1(5S). \tag{10}$$

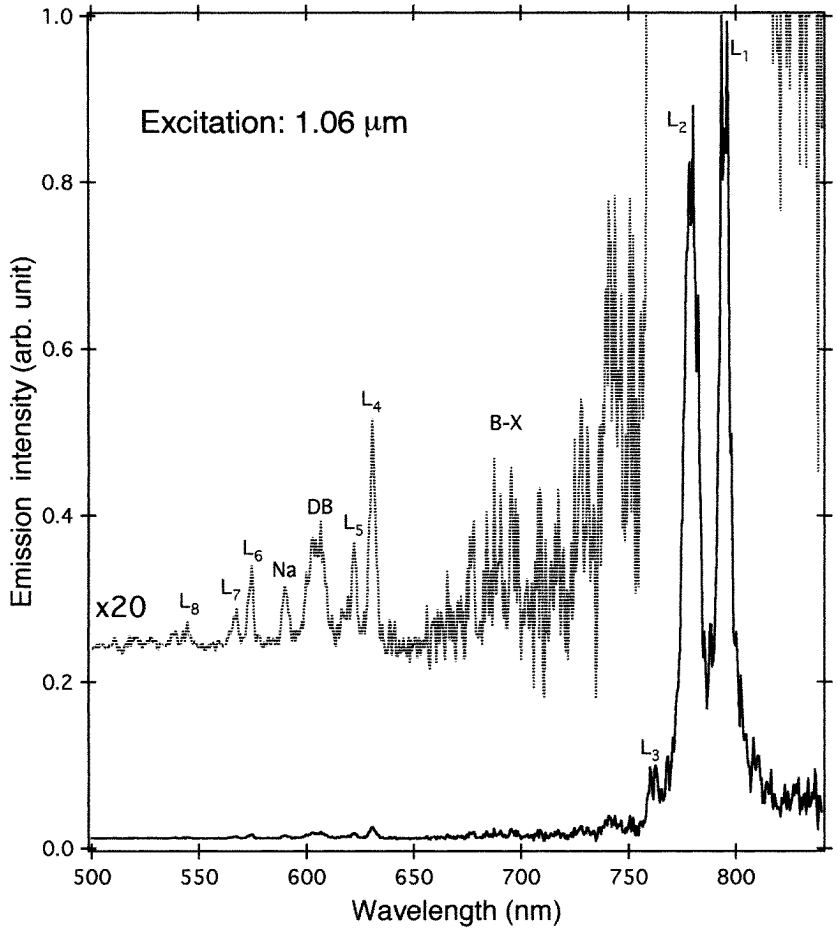

Figure 8. Laser photofragmentation spectra of rubidium vapour zone. The upper curve shows a magnification of the lower one by a factor of 20.

The above excitation-energy transfer and energy pooling may indicate that collisions between vapour species in rubidium vapour occur frequently to produce clusters.

3.4. Laser-induced fragmentation of rubdium vapour and diffuse band emission

We measured the emission spectra of the rubidium vapour in helium atmosphere confined at 150 Torr for different heights after pulsed-laser-light irradiation (laser fluence: about 100 mJ cm^{-2}). The spectra at the height of 5 mm are shown in figure 8. As shown in this figure, we observed sharp lines L_1, L_2, L_3, L_4, L_5, L_6, L_7 and L_8. By referring to the spectroscopic table (Lide 1990–1991), L_1, L_2, L_3, L_6 and L_7 are assigned to electronic transitions in neutral atoms. L_4, L_5 and L_8 are assigned to electronic transitions in singly ionized atoms. Moreover, we observed a broad band at about 690 nm which is assigned to the B–X transition in the rubidium dimer, and another broad band DB at about 605 nm which is assigned to the diffuse band of excimer dimers. This diffuse band was observed only at the final stage of evaporation and the orange colour was visible to the naked eye. The diffuse band emission is attributed to the triplet–triplet Rb_2 $2\,^3\Pi_g \rightarrow 1\,^3\Sigma_u^+$ bound–free transition (Xing *et al* 1992, Luh *et al* 1988).

The observed diffuse band has some structure, which arises from the spin–orbit splitting in the $2\,^3\Pi_g$ state.

The results obtained at various evaporation conditions (atmospheric gas pressure, kind of atmospheric gas and evaporation temperature) are summarized briefly as follows.

(a) In the laser photofragmentation of rubidium vapour, emissions from variously excited atoms, dimers and diffuse band emission are observed.
(b) The spectral features are independent of the kind of atmosphere, but the emission intensity increases when the helium gas is replaced by argon.

The result (a) may be interpreted as follows. Since we used the 1.06 μm laser line for the excitation and the diffuse band emission was only at the final stage of evaporation, only clusters can be photo-excited electronically through the weak absorption at the long-wavelength tail of the collective-mode-resonance band. The energy absorbed in clusters is then distributed to vibrational modes in the clusters and it concentrates in a special vibrational mode to evaporate atoms and smaller clusters because of the small number of degrees of freedom and small heat capacity. However, since the laser pulse duration is long, the smaller clusters evaporated may be subsequently heated optically by the laser and fragment to produce neutral atoms, ionized atoms, dimers, excimer-like $2\,^3\Pi_g$ dimers, neutral trimers, trimer ions and electrons. At present, it is not clear whether the diffuse band emission arises directly from the $2\,^3\Pi_g$ dimers, or via a dissociative recombination process ($Rb_3^+ + e \rightarrow Rb_1$+excimer-like Rb_2). The result (b) indicates that heavier atmospheric gas confines or effectively deexcites the plume.

4. Final remarks and conclusion

In conclusion, we have performed a measurement of the time evolution of extinction spectra of the rubidium vapour zone produced by thermal evaporation both in a confined and flowing noble gas. The time trend of the obtained spectra indicates that Rb_2 is produced by coalescence of Rb_1 and that the surface plasma resonance frequency of rubidium clusters is first blueshifted with increasing cluster size, while, with further increase of cluster size, the frequency becomes redshifted. The main limitation of our technique is that there is no direct characterization of the cluster size, *in situ*. Bearing this limitation in mind, we have presented some reasonable connection between measured optical data and size effects in rubidium clusters and microcrystals.

Also, laser-excitation experiments give some information on the vapour zone, the excitation energy transfer between rubidium vapour species, the structure of the vapour zone and the mechanism of the laser photofragmentation of clusters.

References

Ashcroft N W and Mermin N E 1976 *Solid State Physics* (New York: Holt, Rinehart and Winston)
Barbier J and Cheret M 1983 *J. Phys. B: At. Mol. Phys.* **16** 3213
Brechignac C, Chauzac Ph, Kebaili N, Leygnier N and Sarfati A 1992 *Phys. Rev. Lett.* **68** 3916
Brom J M and Broida H P 1974 *J. Chem. Phys.* **61** 982
Filby J D and Martin D L 1965 *Proc. R. Soc.* A **284** 83
Inoue S T, Asano S and Yamasita J 1971a *J. Phys. Soc. Japan* **30** 1546
——1971b *J. Phys. Soc. Japan* **31** 422
Kreibig U 1974 *J. Phys. F: Met. Phys.* **4** 999
Lide D R 1990/1991 *CRC Handbook of Chemistry and Physics* 71st edn (Boston, MA: Chemical Rubber Company) pp 10–82
Lien W H and Phillips N E 1964 *Phys. Rev.* A **133** 1370

Luh Wei-Tzou, Bahns J T, Lyyra A M, Sando K M, Kreiber P D and Stwalley W C 1988 *J. Chem. Phys.* **88** 2235
Mann D M and Broida H P 1973 *J. Appl. Phys.* **44** 4950
Mochizuki S 1991 *Phys. Lett.* A **155** 510
——1992 *Phys. Lett.* A **164** 191
——1993 *Phys. Lett.* A **176** 382
Mochizuki S and Ruppin R 1993 *J. Phys.: Condens. Matter* **5** 135
——1994 *J. Phys.: Condens. Matter* **6** 7303
Mochizuki S, Sasaki M and Ruppin R 1997 *J. Phys.: Condens. Matter* **9** 5801
Mochizuki S and Tsumura S 1998 *Meeting Abstracts Phys. Soc. Japan* (Tokyo: Physical Society of Japan) part 2, p 357
Pichler G, Milosevic S, Veza D and Beuc R 1983 *J. Phys. B: At. Mol. Phys.* **16** 4619
Phelps F M III 1982 *M. I. T. Wavelength Tables* (Cambridge, MA: MIT Press)
Rosen B 1970 *Spectroscopic Data Relative to Diatomic Molecules* (Oxford: Pergamon)
Selby K, Kresin V, Matui J, Kresin V, Vollmer M, de Heer W A, Scheidermann A and Knight W D 1991 *Phys. Rev.* B **43** 4565
Selby K, Vollmer M, Matui J, Kresin V, de Heer W A and Knight W D 1989 *Phys. Rev.* B **40** 5417
Smith N V 1970 *Phys. Rev.* B **2** 2840
Suemitsu H, Kitaura H, Yokoyama R, Ehara M and Nakatsuji H 1992 *J. Phys. B: At. Mol. Opt. Phys.* **25** 4507
White H E 1934 *Introduction to Atomic Spectra* (New York: McGraw-Hill) p 119
Xing D, Ueda K and Takuma H 1992 *Appl. Phys. Lett.* **60** 2960
Yamashita J 1973 *Kotai Densiron* (Tokyo: Asakura Syotn) (in Japanese)